Molecular Dynamics Simulation of Shearing Deformation Process of Silicon Nitride Single Crystal

ARTICLE *in* COMPUTATIONAL MATERIALS SCIENCE · APRIL 2002

Impact Factor: 2.13 · DOI: 10.1016/S0927-0256(01)00225-7

5 AUTHORS, INCLUDING:

Shigenobu Ogata
Osaka University
120 PUBLICATIONS **2,206** CITATIONS

ELSEVIER

Computational Materials Science 23 (2002) 146–154

COMPUTATIONAL MATERIALS SCIENCE

www.elsevier.com/locate/commatsci

Molecular dynamics simulation of shearing deformation process of silicon nitride single crystal

Shigenobu Ogata [a], Hiroshi Kitagawa [a], Naoto Hirosaki [b,*], Yoshinari Hatanaka [a], Takashi Umezu [a]

[a] *Department of Adaptive Machine Systems, Graduate School of Osaka University, Suita 565-0871, Japan*
[b] *National Institute for Research in Inorganic Materials, 1-1 Namiki, Tsukuba-shi, Ibaraki 305-0044, Japan*

Accepted 1 June 2001

Abstract

Shear deformation properties of α and β silicon nitride single crystals are investigated using the classical molecular dynamics (CMD) method. Four cases of shearing directions are analyzed, which were reported to be slip system on the basis of experimental observations. The simulation results show that shear deformation does not occur in one of the experimentally predicted slips ($\alpha - \{1\bar{1}01\}\ \langle 11\bar{2}0\rangle$). In this case the crystal is broken abruptly under shear deformation. In the case of the β crystal ($\beta - \{10\bar{1}0\}\ \langle 0001\rangle$), a sharp slip with edge dislocation can be found. The dislocation core width and speed are estimated. Finally one of the CMD results is compared with the corresponding first principle density functional calculation results, and it is shown that the validity about shearing CMD simulation of the 3-body interatomic potential was proposed by Vashishta.

Keywords: α-silicon nitride; β-silicon nitride; Slip system; Dislocation; Computer simulation; Molecular dynamics; 3-body potential; Shear strength; Stress–strain curve; First principle density functional calculation

1. Introduction

Recently, silicon nitride has become the focus of industrial development for its superior mechanical properties [1–3]. A significant amount of experimental research regarding the estimation of the mechanical properties and development of the machining technique has been carried out in recent years [4–7]. However, most researchers have treated silicon nitride as a polycrystalline material. The characteristics of the material as a single crystal have not been studied sufficiently [3] because of the difficulty associated with obtaining relatively large specimens. Suematsu et al. [8,9] have recently succeeded in producing a single crystal with a characteristic dimensions of the order of a millimeter size using a chemical vapor deposition process. Thus direct measurement of the mechanical properties of the single crystal is now a possibility.

In addition, computer simulations of the atomic and electron level structural dynamics are also possible due to the significant progress of computing power. The intrinsic elastic constant, lattice constant and atomic arrangement of the silicon

* Corresponding author.
E-mail address: hirosaki@nirim.go.jp (N. Hirosaki).

0927-0256/02/$ - see front matter
PII: S0927-0256(01)00225-7

nitride single crystal have been calculated in detail by using first principle calculations. These calculations are based on the density functional theory and performed by Ching et al. [10] and the linear combination of atomic orbitals (LCAO) method performed by Wendel and Goddard [11]. Furthermore, Vashishta et al. have reported large-scale simulations of the sintering process, and of the mechanical behavior of nanocrystal and amorphous silicon nitride using the classical molecular dynamics (CMD) method by introducing an appropriate interatomic potential [12–16]. Several empirical and semi-empirical interatomic potentials have been proposed for the effective CMD simulations of silicon nitride [11,12,17].

Although silicon nitride is generally classed as a polycrystalline material, it is important to know the intrinsic properties as a single crystal, in order to characterize material strength and deformation. The tensile fracture properties of the single crystal have been evaluated using an atomic simulation method [18]. In this paper we will investigate shear deformation and discuss the evident slip mechanisms.

It is known that silicon nitride has two phases, called α and β silicon nitride. Niihara and Hirai [2] performed Knoop hardness test for the α phase single crystal and reported that $\{10\bar{1}0\}\ \langle 0001\rangle$ is the primary slip system. On the other hand, Suematsu et al. [19] asserted that the $\{1\bar{1}01\}\ \langle 11\bar{2}0\rangle$ is the primary slip system, from the results of Knoop hardness tests and the transmission electron microscope (TEM) observation of the plastically deformed single crystal. This contradiction in the reported experimental observations of the primary slip system has not yet been resolved. For β crystal, Evans et al. [1], Kawahara et al. [20] and Milhet et al. [21] have reported that $\{10\bar{1}0\}$-$\langle 0001\rangle$ is the primary slip system. Kawahara et al. have also reported that the $\{10\bar{1}0\}\ \langle 1\bar{2}10\rangle$ is the secondary slip system.

Ogata et al. [23,24] performed a molecular dynamics simulation of shearing deformation for the α and β single crystal, and examined the ideal shear strength and the validity of the experimentally determined slip systems. They predicted a slip mechanism at the atomic scale and an ideal shear strength of the single crystals. The workers suggested that there is a possibility that slip deformation occurs by dislocation in a slip system of β crystal. However, in this simulation the periodic boundary condition (PBC) in the direction parallel to the slip plane strongly restricts deformation in the model. As a result, it may be difficult to observe any dislocation. In this paper, we used the CMD model that does not take the PBC in direction parallel to the slip plane. Furthermore, the accuracy of the 3-body interatomic potential is estimated by the comparison with the result of the first principle density functional calculation.

2. Interatomic potentials for MD simulation

We introduce the interatomic potential functions proposed by Vashishta et al. [25], which consists of 2-body ($V_{ij}^{(2)}$) and 3-body ($V_{jik}^{(3)}$) interaction terms. The total potential energy of the system (E) can be calculated by

$$E = \sum_{i<j} V_{ij}^{(2)}(r_{ij}) + \sum_{i,j<k} V_{jik}^{(3)}(r_{ij}, r_{ik}, \theta_{jik}), \tag{1}$$

where i, j, and k are labels of the atoms of the system, r_{ij} is the length of the ij bond, and θ_{jik} is the bond angle between bonds ij and ik. The functions $V_{ij}^{(2)}(r_{ij})$ and $V_{jik}^{(3)}(r_{ij}, r_{ik}, \theta_{jik})$ are expressed by

$$V_{ij}^{(2)}(r_{ij}) = A_{ij}\left(\frac{\sigma_i+\sigma_j}{r_{ij}}\right)^{\eta_{ij}} + \frac{Z_iZ_j}{r_{ij}}\exp\left(-\frac{r_{ij}}{r_{s1}}\right) - \frac{\alpha_iZ_j^2+\alpha_jZ_i^2}{2r_{ij}^4}\exp\left(-\frac{r_{ij}}{r_{s4}}\right) \tag{2}$$

and

$$V_{jik}^{(3)}(r_{ij}, r_{ik}, \theta_{jik}) = B_{jik}\exp\left(\frac{l}{r_{ij}-r_c}+\frac{l}{r_{ik}-r_c}\right) \times (\cos\theta_{jik} - \cos\theta_{jik}^0), \tag{3}$$

where $A, \sigma, \eta, Z, r_{s1}, \alpha, r_{s4}, B, l, r_c, \theta^0$ are the parameters. These parameters were determined by Vashishta et al. [25] for silicon nitride.

The 2-body potential function consists of terms representing repulsion, Coulomb interaction, and charge dipole interaction caused by the strong electronic polarizability. The 3-body function is made up of the bond bending terms due to the covalent nature of the bonds. The above expression

for the interatomic potential has been already applied to various MD calculations and is known to give excellent results, for the equilibrium lattice parameters, elastic constants, phonon density of states and specific heat, in comparison with the experimental data [26,27].

3. Model

Four types of shear deformation are analyzed to examine the properties of the slip system, that is, $\alpha - \{1\bar{1}01\}\ \langle 11\bar{2}0\rangle$ (Case 1), $\alpha - \{10\bar{1}0\}\ \langle 0001\rangle$ (Case 2), $\beta - \{10\bar{1}0\}\ \langle 0001\rangle$ (Case 3), and $\beta - \{10\bar{1}0\}\ \langle 1\bar{2}10\rangle$ (Case 4). The Cases 1 and 2 correspond to the possible primary slip systems which were reported by Suematsu et al. [19] and Niihara and Hirai [2], respectively. Cases 3 and 4 correspond to the primary slip systems which were reported by Evans et al. [1], Kawahara et al. [20] and Milhet et al. [21].

A schematical diagram and the dimensions of the model are shown in Fig. 1 and Table 1, respectively. The same model was used by Gumbsch et al. [22] to simulate dislocation in a metal. The z-axis is taken in the normal direction to the slip plane and the x-axis parallel to the slip direction. Periodic boundary conditions are applied only in the y-direction. The atoms in region B are fixed and in region A are rigidly shifted toward the x-direction. The sliding speed is assumed to be 10 m/s. The atoms in the region C are restricted and can only move in the x-direction. It must be noted that l must be relatively large since the sliding process does not depend on the boundary conditions. We selected a suitable value for l for each case from our previous work [23,24]. The applied values of l are listed in Table 1 for each case.

Before shear deformation is induced, the model is relaxed for 0.6 ps under an initial temperature using Nośe's thermostat algorithm [28]. After this, Nośe's thermostat is removed and shear deformation is added by setting the sliding speed along the slip direction. For the initial temperature of the simulation room temperature is selected: 300 K. The time increment of the numerical integration of the equations of motion is set at 0.3 fs.

4. Results and discussions

Snapshots of the atomic arrangement in the model under shear deformation are shown in Figs. 2–5. The black and gray circles represent nitrogen

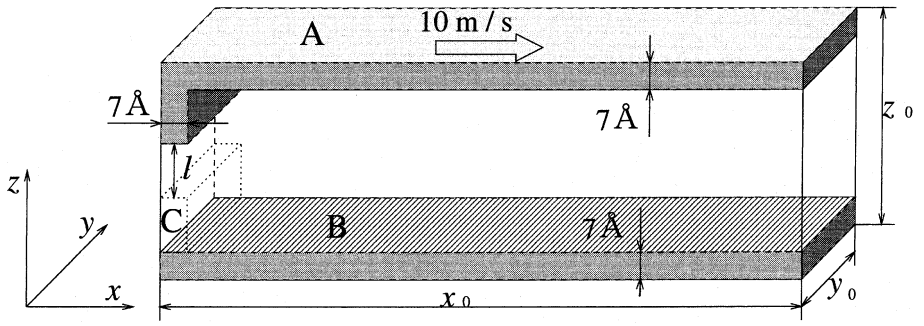

Fig. 1. Schematic illustration of a model for silicon nitride sliding simulation and boundary conditions.

Table 1
Dimensions of models; all parameters are defined in Fig. 1

	Total number of atoms	x_0 Å × y_0 Å × z_0 Å	l, Å
Model for Case 1	7740	117.2×17.6×40.0	16.8
Model for Case 2	10 920	111.8×23.4×43.3	10.8
Model for Case 3	3920	87.1×22.8×21.0	1.0
Model for Case 4	10 080	113.9×17.4×52.6	12.6

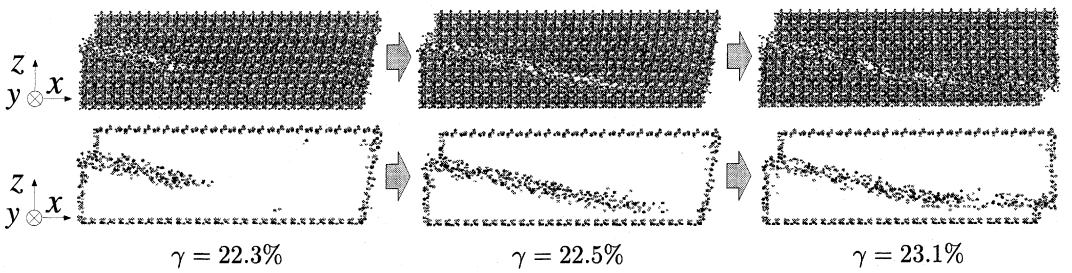

Fig. 2. Atomic configuration (upper) and atoms which have different coordination numbers from perfect crystal (lower) under shear deformation for Case 1. The black and gray circles represent the nitrogen and silicon atoms, respectively.

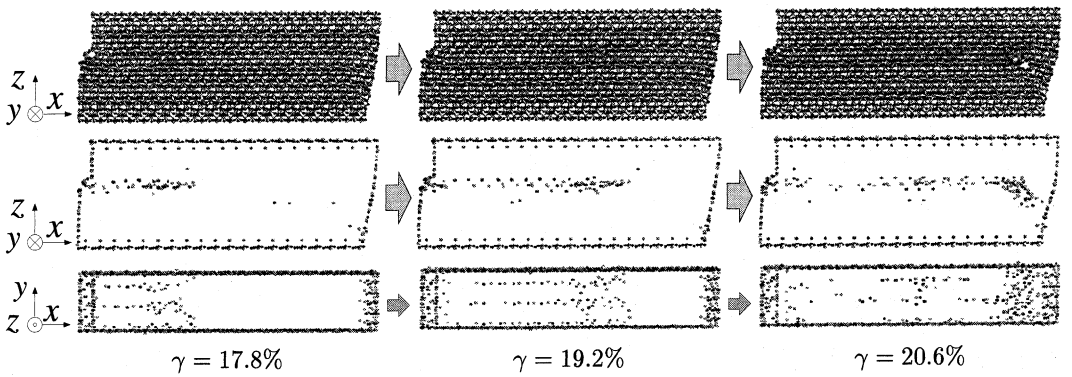

Fig. 3. Atomic configuration (upper) and atoms which have different coordination numbers from perfect crystal (middle and bottom) under shear deformation for Case 2. The black and gray circles represent the nitrogen and silicon atoms, respectively.

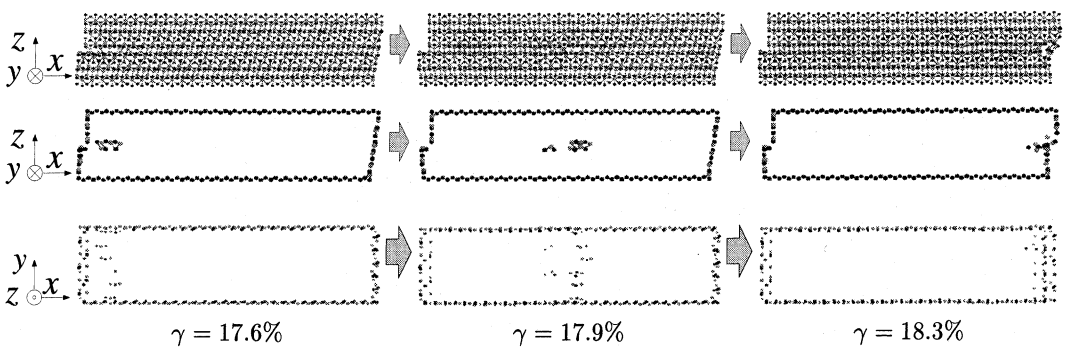

Fig. 4. Atomic configuration (upper) and atoms which have different coordination numbers from perfect crystal (middle and bottom) under shear deformation for Case 3. The black and gray circles represent the nitrogen and silicon atoms, respectively.

and silicon atoms, respectively. The upper figures show atomic configurations observed in the y-direction and the middle figures show special atoms also observed in the y-direction. In the model the atoms have a coordination number which differs from that of perfect crystal. The lower figures show the atoms which also have a different coordination number to perfect crystal and exist near the sliding plane. These figures are viewed from the z-direction. However, the last figure for the Case 1

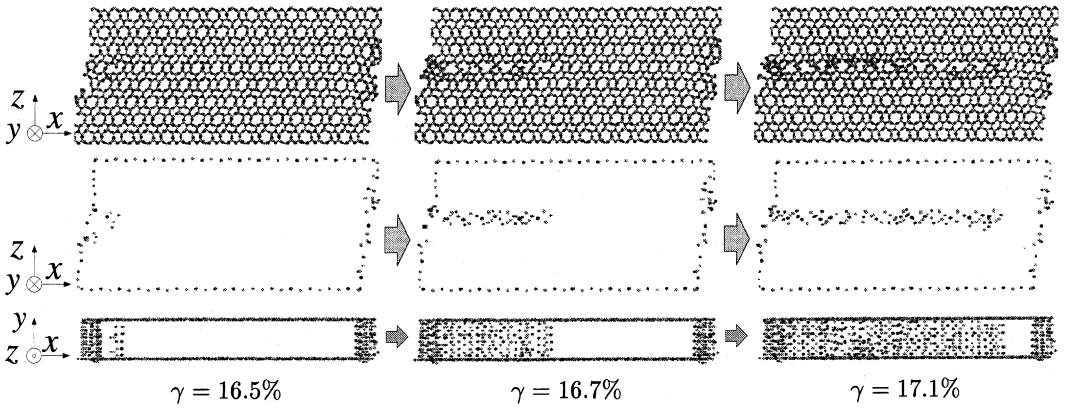

Fig. 5. Atomic configuration (upper) and atoms which have different coordination numbers from perfect crystal (middle and bottom) under shear deformation for Case 4. The black and gray circles represent nitrogen and silicon atom, respectively.

is omitted, because the slip plane cannot be defined from the results in this case. The corresponding shear stress–strain curve and potential energy–strain curve are shown in Figs. 6–9. The shear strain γ is calculated as the sliding displacement per unit height of the model excluding the lower fixed and the upper sliding regions. The shear stress σ is calculated as the sum of all the atomic forces of the fixed atoms along the shear direction divided by the initial area of the sliding plane.

4.1. Case 1

In this case, plastic deformation along the sliding direction was not observed. However, Suematsu et al. [19] asserted that this direction is one of the slip systems. Therefore, we are not able to confirm that slip occurs in this direction. From Fig. 6, it is clear that elastic behavior was observed up to a stress level of 25 GPa. It was found that the stress and potential energy decreased sharply when the stress reached 25 GPa, because brittle fracture occurs in the crystal as shown in Fig. 2. Thus, elastic behavior is only observed for stresses below 25 Gpa.

4.2. Case 2

As shown in Fig. 7, the model deforms elastically up to a stress level of 20 GPa, and then the stress gradually decreases up to a strain level of 21%. Above this strain level, the shear stress begins to increase elastically. It is assumed that the plastically deformed region is limited to a narrow re-

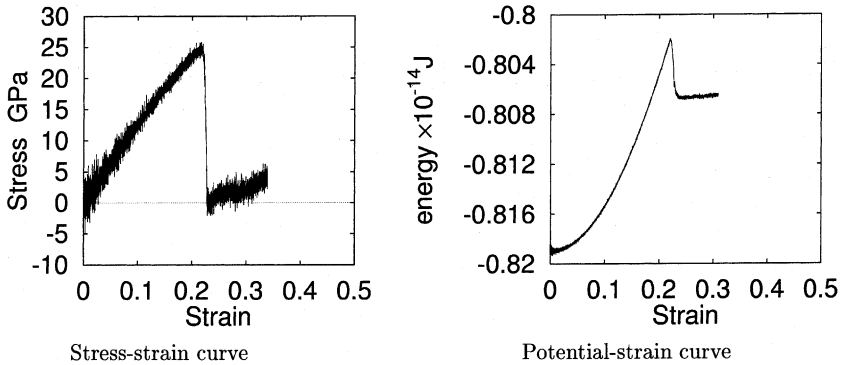

Fig. 6. Stress–strain curve and potential energy–strain curve of Case 1.

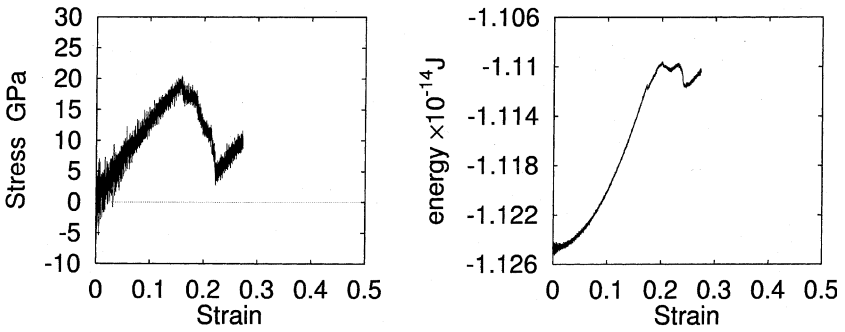

Stress-strain curve Potential-strain curve

Fig. 7. Stress–strain curve and potential energy–strain curve of Case 2.

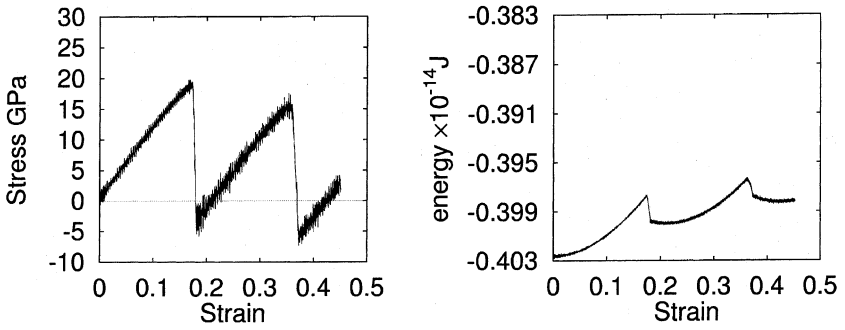

Stress-strain curve Potential-strain curve

Fig. 8. Stress–strain curve and potential energy–strain curve of Case 3.

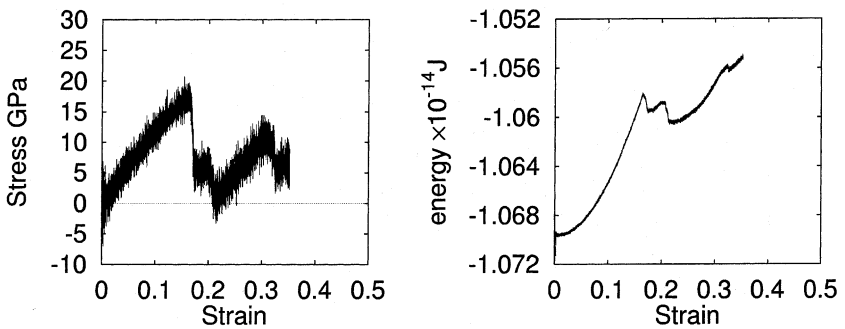

Stress-strain curve Potential-strain curve

Fig. 9. Stress–strain curve and potential energy–strain curve of Case 4.

gion near the slip plane. As the stress decreases, the region of disordered atomic structure moves to the right edge from the left like a dislocation. However, the speed is much lower than the speed of sound. The atomic structure after the disordered region has moved is almost the same as the initial atomic structure, as shown in the middle and bottom illustrations of Fig. 3.

4.3. Case 3

In this case, the slip progresses by dislocation moving as shown in Fig. 4. The width of the dislocation is estimated to be approximately 8 Å. From Fig. 8 it is seen that the system is elastically deformed up to a stress level of 18.5 GPa, and then the stress abruptly decreases. While the stress is decreasing, the dislocation moves to the right edge from the left. Following this, elastic behavior is observed once again. A negative stress level is obtained and is shown in Fig. 8. This is due to a negative residual shear elastic deformation of the lower region of the model. This condition is supported from the result obtained at the strain level of $\gamma = 17.9\%$, shown in Fig. 4.

4.4. Case 4

In this case, the first slip occurs at a stress level of 17 GPa. A rebonding process zone on two or three atomic layers around the slip plane moves to the right edge from the left. This process is the cause of the slip deformation. The other atomic layer exhibits the initial crystal structure and no plastic deformation is observed. The second slip occurs at a stress level of 10 GPa, which is lower than that of the first slip of 17 GPa. This is due to a disordered region near the slip plane which induces the decreasing crystal strength.

4.5. Estimation of reliability of interatomic potential

To examine the validity of the 3-body potential for the investigation of shearing properties, the result obtained using the 3-body potential is compared with that given by the first principle density functional calculation. The calculation model cell is shown in Fig. 10. The x-, y- and z-directions are set to be the $\langle 1\,0\,0\,0\rangle$, $\langle 0\,1\,\bar{1}\,0\rangle$ and $\langle 0\,0\,0\,1\rangle$ directions of the β crystal, respectively. This model contains 84 atoms, with the dimensions of model shown in Fig. 10.

A shear deformation is applied by means of a rigid step sliding procedure of the model center region as shown in Fig. 11. The sliding direction and slip plane orientation correspond to those of

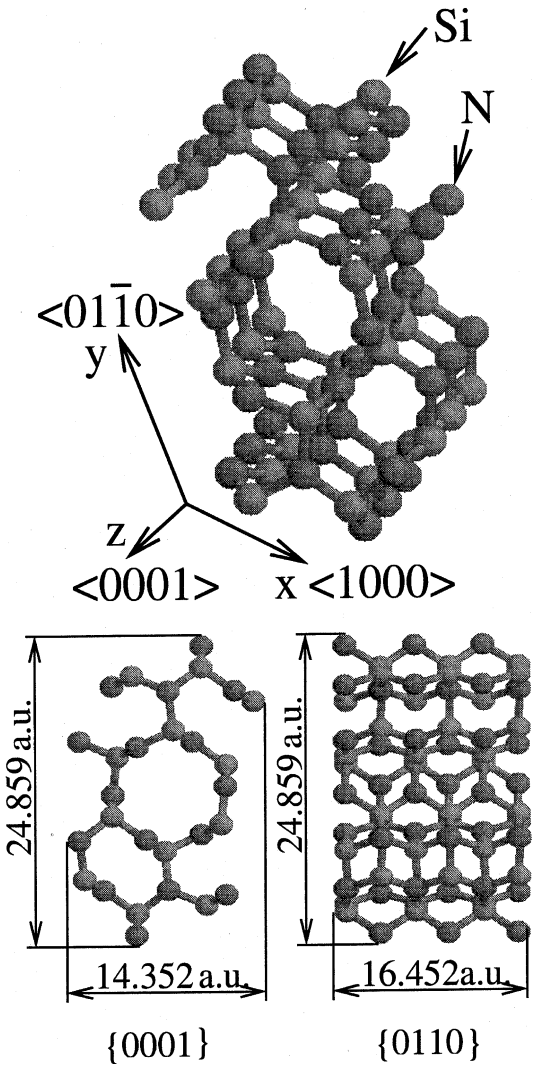

Fig. 10. Super cell model for estimation of the reliability of interatomic potential.

Case 3 discussed previously. The sliding step is set to be 0.34275 a.u., which corresponds to the 1/16 of the c lattice constant. The PBC is applied along the x-, y- and z-directions. In this calculation, atomic structure relaxation is not performed. The plane wave cut-off energy of 36 Ry and four k-points $(1/4, 0, 1/4), (-1/4, 0, 1/4), (1/4, 0, -1/4), (-1/4, 0, -1/4)$ are used for the first principle calculation. The total energy differences from the initial energy are estimated by first principle calculation and the 3-body potential.

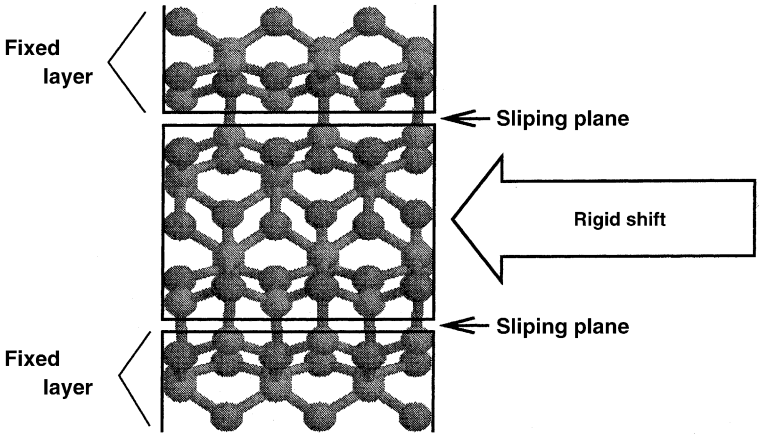

Fig. 11. Method of appling shear deformation.

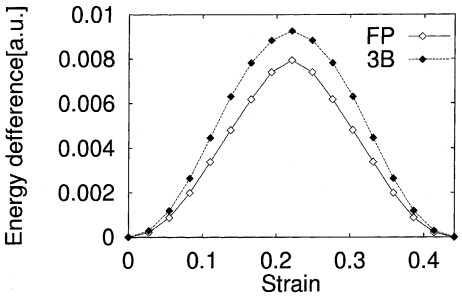

Fig. 12. Potential energy change in sliding process estimated by first principle calculation and 3-body potential.

Potential energy difference – strain curves are shown in Fig. 12. The results obtained from the 3-body potential are in good agreement with those of the first principle method qualitatively. It is found that the 3-body interatomic potential is valid for the modeling of the shear process. From this calculation, the ideal shear strength can be estimated at approximately 22 GPa using the first principle method and 28 GPa using the 3-body potential.

5. Conclusion

Molecular dynamics analyses of shearing deformation of the α and β silicon nitride single crystals have been performed and the mechanical properties for shear deformation have been examined. The main results obtained are summarized as follows:

1. The shear strength for the $\alpha - \{1\bar{1}01\}\ \langle 11\bar{2}0\rangle$ is highest and those for $\alpha - \{10\bar{1}0\}\ \langle 0001\rangle$ (Case 2), $\beta - \{10\bar{1}0\}\ \langle 0001\rangle$ (Case 3), and $\beta - \{10\bar{1}0\}\ \langle 1\bar{2}10\rangle$ (Case 4) are from 18 to 20 GPa.
2. Failure occurs under the $\{1\bar{1}01\}\ \langle 11\bar{2}0\rangle$ shear deformation for α single crystal, and no shear plastic deformation is observed.
3. Dislocation appears under the $\{10\bar{1}0\}\ \langle 0001\rangle$ shear deformation for β single crystal.
4. Localized band-like shear deformation occurs under $\{10\bar{1}0\}\ \langle 0001\rangle$ α single crystal and $\{10\bar{1}0\}\ \langle 1\bar{2}10\rangle$ for β single crystal.
5. The $\alpha - \{10\bar{1}0\}\ \langle 0001\rangle$ (Case 2), $\beta - \{10\bar{1}0\}\ \langle 0001\rangle$ (Case 3), and $\beta - \{10\bar{1}0\}\ \langle 1\bar{2}10\rangle$ (Case 4) systems are intrinsically prone to slip.
6. From the comparison with the first principle calculation, it is found that the 3-body potential proposed by Vashshita et al. results in a good estimation of the shear deformation properties.

References

[1] A.G. Evans, J.V. Sharp, J. Mater. Sci. 6 (1971) 1292–1302.
[2] K. Niihara, T. Hirai, J. Mater. Sci. 14 (1979) 1952–1960.

[3] H. Suematsu, J.J. Petrovic, T.E. Mitchell, J. Ceram. Soc. Jpn. 105 (1997) 842–846 (in Japanese).
[4] K. Hatanaka, H. Shiota, T. Ando, Trans. Jpn. Soc. Mech. Eng. A 56 (1990) 317–324 (in Japanese).
[5] H. Hohjo, H. Shibata, N. Kamiya, A. Otsuka, T. Miyata, J. Soc. Mater. Sci. Jpn. 46 (1997) 282–287 (in Japanese).
[6] H. Sato, M. Mitomo, T. Nishimura, H. Emoto, J. Ceram. Soc. Jpn. 106 (1998) 203–207 (in Japanese).
[7] Y. Mochida, T. Nishioka, A. Yamakawa, Y. Tanaka, Y. Ogura, H. Nakao, M. Miyake, J. Ceram. Soc. Jpn. 105 (1997) 784–788.
[8] H. Suematsu, J.J. Petrovic, T.E. Mitchell, in: I.W. Chen, P.F. Becher, M. Mitomo, G. Petzow, T.S. Yen (Eds.), Silicon Nitride Ceramics, Mater. Res. Soc. Symp. Proc. 287 (1993) 449–454.
[9] H. Suematsu, M. Mitomo, T.E. Mitchell, J.J. Petrovic, O. Fukunaga, N. Ohashi, J. Am. Ceram. Soc. 80 (1997) 615–620.
[10] W.Y. Ching, Y-N. Xu, J.D. Gale, M. Rühle, J. Am. Ceram. Soc. 81 (1998) 3189–3196.
[11] J.A. Wendel, W.A. Goddard III, J. Chem. Phys. 97 (1992) 5048–5062.
[12] P. Vashishta, R.K. Kalia, I. Ebbsjö, Phys. Rev. Lett. 75 (1995) 858–861.
[13] P. Vashishta, A. Nakano, R.K. Kalia, I. Ebbsjö, J. Non-Cryst. Solids 182 (1995) 59–67.
[14] K. Tsuruta, A. Omeltchenko, R.K. Kalia, P. Vashishta, Europhys. Lett. 33 (1996) 441–446.
[15] R.K. Kalia, A. Nakano, K. Tsuruta, P. Vashishta, Phys. Rev. Lett. 78 (1997) 689–692.
[16] R.K. Kalia, A. Nakano, A. Omeltchenko, K. Tsuruta, P. Vashishta, Phys. Rev. Lett. 78 (1997) 2144–2147.
[17] F.B. Mota, J.F. Justo, A. Fazzio, Phys. Rev. B 58 (1998) 8323–8328.
[18] N. Hirosaki, S. Ogata, H. Kitagawa, Mater. Sci. Res. Int. 5 (1999) 253–257.
[19] H. Suematsu, J.J. Petrivic, T.E. Mitchell, Mater. Sci. Eng. A 209 (1996) 97–102.
[20] K. Kawahara, S. Tsurekawa, H. Nakashima, J. Jpn. Inst. Metals 60 (1996) 582–588.
[21] X. Milhet, H. Garem, J.L. Demenet, J. Rabier, T. Rouxel, J. Mater. Sci. 31 (1997) 3733–3738.
[22] P. Gumbsch, H. Gao, Science 283 (1999) 965–968.
[23] S. Ogata, H. Kitagawa, N. Hirosaki, H. Yasumoto, Mater. Trans. JIM 40 (1999) 1262–1268.
[24] S. Ogata, H. Kitagawa, N. Hirosaki, H. Yasumoto, J. Soc. Mater. Sci. Jpn. 49 (2000) 257–262.
[25] R. Vashishta, R.K. Kalia, A. Nakano, I. Ebbsjö, in: M.F. Thorpe, M.I. Mitkova (Eds.), Amorphous Insulators and Semiconductors, Kluwer Academic Publishers, Dordrecht, MA, 1996, pp. 151–213.
[26] C.K. Loong, P. Vashishta, R.K. Kalia, I. Ebbsjö, Europhys. Lett. 31 (1995) 201–206.
[27] A. Nakano, R.K. Kalia, P. Vashishta, Phys. Rev. Lett. 75 (1995) 3138–3141.
[28] S. Noše, J. Chem. Phys. 81 (1984) 511–519.